Peer-reviewed version available at *Geosciences* **2018**, *8*, 215; doi:10.3390/geosciences8060215

Fracture and lineament patterns across the Midcontinent indicate post-Cretaceous reactivation of basement-involved faults

C.M. Burberry[1*] & J. L. Swiatlowski[1,2] & M.L. Searls[1] & I. Filina[1]

[1]University of Nebraska-Lincoln; [2]University of California, Riverside.

*corresponding author; cburberry2@unl.edu

ABSTRACT

Reactivation of pre-existing weaknesses in the upper crust can be documented using surface features, and has occurred throughout time and space, particularly in regions where the basement material dates from the Precambrian and has undergone successive deformation events. This study aims to use surface features such as fracture patterns to document evidence of such reactivation in the Paleozoic and Cenozoic of Nebraska and Kansas (units separated by an unconformity in the study area). The most prominent basement features in southeast Nebraska and northeast Kansas are oriented NE-SW, likely related to the midcontinent rift, and oriented NW-SE, likely related to fabrics from the Central Plains Orogen. These features are well defined in the potential fields data. Fracture patterns in the study area show an E-W oriented trend, as well as clearly discernable NE-SW and subsidiary N-S and NW-SE trends. The E-W trend is interpreted to be related to far-field stresses from Laramide and Ancestral Rocky Mountain orogenic events, whilst the NE-SW trend is interpreted to be related to subtle reactivation on the Mid-continent rift and related faults, observed in basement data. These movements produced stresses of sufficient magnitude to produce extensional fractures in the overlying rock units, but not sufficient to generate shear. Similarly, the ~N-S and NW-SE fracture trends are taken as evidence of subtle reactivation on the Nemaha Uplift and Central Plains Orogen systems, generating fractures but not shear movement. This contribution therefore provides a convincing case-study of the value of fracture orientations (that is, surface morphodynamics) in discerning buried tectonic trends and subtle reactivation thereon.

KEYWORDS: fractures; potential fields; lineament analysis; fault reactivation; Midcontinent rift system; Nemaha uplift

1.INTRODUCTION

In many landscapes, surface evidence of deformation can provide a tantalizing glimpse of the structures beneath the surface. Landscape maturity can be used to determine the order in which folds amplified and to discern the presence of subtle folding structures that cannot be observed in other ways (e.g. Obaid & Allen, 2017). Landslide occurrence and the relief of the local topography can also be employed to understand the pattern of active faults in a region (e.g. Osmundsen et al., 2009). Cinque et al. (1993) use geomorphological domains in addition to subsurface datasets to infer the geodynamic evolution of the Southern Apennines. These three diverse studies highlight the importance of geomorphologic data in subsurface geology. In this contribution, we use the shape of the land surface, as gleaned from satellite data and field-derived fracture patterns, to understand the reactivation history of basement-involved faults in SE Nebraska and NE Kansas.

Reactivation of pre-existing weaknesses in crustal material is documented throughout time and space, particularly in regions where the basement material dates from the Precambrian and has undergone successive episodes of deformation. The concept of tectonic inheritance - that the pre-existing structures and zones of weakness in a system govern the development of subsequent structures - is frequently used to explain large-scale variations in the geometry of orogenic belts, or the locations of rift margins in supercontinent cycles (Butler et al., 1997, Thomas 2004, Audet & Burgmann, 2011, Huerta & Harry, 2012). In addition, this concept can be used to explain the appearance of folds and faults or uplifted zones in regions that are far from the collision zone. The effect of basement geometry on the development of an orogenic arc has been demonstrated by Macedo & Marshak (1999) using analog models. Large-scale finite-element modeling also demonstrates that a pre-existing structural system can exert significant control on subsequent deformation styles (Huerta & Harry, 2012). Studies of specific structures (e.g. Gates & Costa, 1998; Molliex et al., 2010; Said et al., 2011; McMechan, 2012; Burberry, 2015) indicate that subsequent structures, facies changes and economic deposits may be affected by the motion of the pre-existing fault or faults.

Failed rifts and ancient suture zones can provide weak zones suitable for reactivation in successive deformation events. The amount of reactivated movement seen on any given fault is a function of the

lithospheric strength, number of faults within the sequence, and obliquity between the fault orientation and compression direction (Dewey 1989, Williams et al. 1989, Del Ventisette et al. 2006). Pressure and temperature of the deforming system may also affect reactivation potential (Ranalli, 2000). Major reactivated faults have a mix of effects, such as compartmentalizing the overlying thrust belt structure, nucleating overlying folds, as well as affecting the basement geometry (Butler et al. 2006). Depending upon the compression direction, initially normal faults may be reactivated as strike-slip or as reverse/thrust faults in subsequent deformation if the conditions are correct, that is, the incident stress is within a suitable angle relative to the original fault (Handin, 1969). Some studies indicate that an oblique subsequent imposed stress is more favorable for fault reactivation than an imposed stress normal to the structure (Sibson, 1985). Faults may be reactivated numerous times if the region is affected by multiple phases of deformation, assuming that the above conditions are met in each phase. The effect of an imposed stress on a pre-existing weakness in a specific area can be tested using analog models, where the initial conditions can be chosen and scaled to represent a real-world scenario (McClay, 1995). This methodology has been applied successfully to regions including the Italian Alps and the Zagros Belt (Bahroudi & Koyi, 2003; Viola et al., 2004).

This study aims to demonstrate that basement structures can reactivate and propagate through a thick sequence of cover rocks to influence surface fracture patterns. The study area chosen is the southeastern section of Nebraska and the adjacent northwestern region of Kansas (Figure 1). This area was chosen because there are undisputed structures within the basement namely the southern extent of the Mid-continent Rift System and the northern extent of the Nemaha uplift. Through a comparison of lineaments derived from potential fields processing and analysis, remotely sensed lineaments and surface fracture patterns, we demonstrate that reactivation of basement faults is able to explain the distribution of surface lineaments (that is, probable faults and fractures) in the study area. Previous studies have documented fracture patterns across parts of the present study area (e.g. Neff, 1949; Ward, 1968) and noted the relationship of the surface lineaments to presumed basement features (e.g. Baehr, 1954; Smith et al., 1974; White, 1990). Although providing valuable data, these previous studies cover only a small portion of the present focus area, and lack the understanding of modern rock mechanics in explaining their findings (e.g. Neff, 1949; Nelson, 1952). This study serves to emphasize the influence of basement feature reactivation on surface geomorphology in the framework of modern rock mechanics, and conversely, the importance of surface features in deciphering the history of a region.

2. GEOLOGIC SETTING

The earliest crust in southeast Nebraska and northern Kansas is considered to date from the Central Plains Orogen (CPO trend on Figure 2) around 1.9-1.7 Ga (Carlson, 1995). This crust is crystalline basement, in the area of interest, this is quartzite with granite intrusions (e.g. Jewett & Merriam, 1959; Anderson & Wells, 1968). The study area is dissected by two major structures, the NE-SW trending, 1.1 Ga Mid-Continent Rift System (MRS) and the NNE-SSW trending 300 Ma Nemaha Uplift (NU), as can be seen on contour maps of the top-Precambrian unconformity (e.g. Jewett & Merriam, 1959; Condra & Reed, 1959) and the present Figure 2. The MRS is considered an aulacogen, and has a counterpart failed rift arm to the east. The Nebraska segment of the MRS parallels fabrics within the earlier Central Plains Orogen (Carlson, 1995). In the southern part of the study area, within eastern Kansas, the MRS is cut by a series of NW-SE trending dextral strike-slip faults, on which there have been historical earthquakes (Baars, 1992; Carlson & Treves, 2005). These faults appear to form an accommodation zone between the Nebraskan and Kansan segments of the MRS (Figure 2) and may be related to the boundary of the Central Plains Province or the suture between this province and the Penokean province which is located to the southeast of the MRS (Carlson, 1995, 1997; Berendsen, 1997). The structures are also aligned along the same trend as the Missouri Gravity Low which underlies the accommodation zone as well as additional NW-SE trending lineaments interpreted from gravity and magnetic data (Atekwana, 1996). More detailed maps correlate specific trends to accretion of numerous terranes during the Central Plains Orogen (Carlson, 2007; Whitmeyer and Karlstrom 2007).

The effects of local tectonics during the Infracambrian and the Paleozoic are observed from stratigraphic relationships, thickness changes and multiple unconformities within the Cambrian-Permian succession, particularly in the present study area (Figure 3; Anderson & Wells, 1968; Carlson, 1997, 1998; Burberry et al., 2015). The Cambrian-Devonian succession is chiefly composed of dolomite, with some clastic units; these clastic materials may indicate periods of land exposure and influx of eroded material to an area otherwise covered by a shallow sea (Jewett & Merriam, 1959; Scotese & Golonka, 1992). Subsequently, extensive Mississippian carbonate rocks were deposited in a shallow sea, across large swathes of the midcontinent (Goebel, 1968). The boundary between the Mississippian and the Pennsylvanian rocks is marked by a regional unconformity, showing widespread uplift of the region in the late Mississippian and early Pennsylvanian (e.g. Scotese & Golonka, 1992).

Inversion via compression of MRS system structures is documented from calcite strain analysis in the Lake Superior Region, ranging in age from Grenvillian-age transpressive strain to Permian age contraction

(Craddock et al., 1997). Hauser (1996) also documents Grenville-age inversion on the MRS and cross-sections after Eardley (1962) and Jewett & Merriam (1959) show significant deformation in the Cambrian-Mississippian section, overlain by a base Pennsylvanian unconformity. A major tectonic event, making the NU emergent, is documented in the Ordovician (Anderson & Wells, 1968; Berendsen and Speczik, 1991; Berendsen et al., 1992). The Kansas segment of the MRS may have been reactivated in the latter part of the Paleozoic, forming the Abilene, Voshell, Barneston, and Nemaha anticlines along the eastern edge of the MRS (Mendenhall, 1958; Carlson, 1995). Rift segments are also considered to be reactivated in the formation of the Union fault and related faults of the study area (Carlson, 1997; Burberry et al., 2015). Many workers (e.g. Baars, 1992; Wilson & Berendsen, 1998) consider the NU to be a reactivated fault that originated as part of the MRS, affected by the segmented nature of the rift and the difference in rift orientation between Nebraska and Kansas (Carlson, 1997). The Nemaha uplift is imaged by a COCORP line as a 40 km wide uplift, bounded to the east by the near-vertical Humboldt Fault (Brown et al., 1983; Serpa et al., 1989; Gay, 1999). The Humboldt fault is thought to be a multiply reactivated structure originally related to the MRS, currently showing a transpressive sense of motion (Moore, 1926; Gay, 1999).

The predominant bedrock in the study area is of Pennsylvanian and Permian age. The Pennsylvanian strata are represented by the mixed clastic and shallow-water carbonate facies of the Desmoinesian, Missourian and Virgilian series (Figure 3; Heckel, 2008). The lowermost Pennsylvanian Atokan series is not expected to be present in the study area (Condra & Reed, 1959). The Virgilian Series of the Upper Pennsylvanian (Figure 3) is the oldest material that crops out in the study area (Figure 1; Heckel 2013). The Virgilian series is characterized by 11 of the short, intense highstand interglacials (Heckel, 2008) that make up the Middle and Upper Pennsylvanian. Each of these cyclothems consists of a black-gray shale unit, overlain by a marine limestone consisting of regressive then shoaling upwards facies, overlain by paleosol (Heckel, 2008). Despite the regular presence of shale members in the cyclothems, the net shale is sufficiently low that the shale layers do not act as detachment units (Condra & Reed, 1959; Jewett & Merriam, 1959). Both the Wolfcampian and Leonardian Series of the Lower Permian crop out in the study area (Figure 1). The Wolfcampian series continues the cyclothem succession from the Upper Pennsylvanian (Moore, 1964) and indicates that the Midcontinent Sea (Heckel 2008) still covered the area. The Leonardian Series is made up from dominantly clastic units, including thin anhydrite layers (Condra & Reed, 1959; Jewett & Merriam, 1959; West et al., 2010). This study samples sites from the carbonate units of the Wolfcampian cyclothems, and does not sample the clastic series.

Thickness changes in the Pennsylvanian and Permian sediments around the NU (e.g. Burberry et al., 2015) indicate active tectonics during this period, probably as a result of the Ancestral Rocky Mountain Orogen (ARM: Moore, 1926; Kluth & Coney, 1981; Gay, 1999; Joeckel et al., 2007). This orogeny is a result of the combined stresses on the intraplate region from the contemporaneous Antler orogeny to the west and the Ouachita-Marathon orogeny (i.e. the docking of Gondwana) to the south-east. In support of the reactivation on the NU during the Pennsylvanian-Permian, Merriam & Forster (2002) and Underwood and Poison (1988) document a series of earthquake proxy locations, including intraformational faulting and contorted bedding in the Pennsylvanian and Permian section.

Following significant uplift and exposure during the Triassic and Jurassic, the region formed part of the shoreline of the Cretaceous Western Interior Seaway during the Late Cretaceous. This period is marked by the deposition of the Dakota Group (Condra & Reed, 1959; Jewett & Merriam, 1959). No Triassic or Jurassic age rocks are recorded in the study area (Figure 1). The Dakota Group includes alternating reddish, clay-rich paleosols and clean, cross-bedded sandstone units, some of which were sampled at sites NF 1, NF 2 and KF 1. Overlying the Dakota group is the Graneros Shale and the Greenhorn Formation, representing periods of incursion of the Seaway and deposition of shales, followed by the thinly-bedded carbonate and shale layers of the Greenhorn Formation (Condra & Reed, 1959). The Greenhorn Formation is sampled at location KF 2 and is the youngest Formation sampled in this study.

After the ARM-related reactivation pulses, the NU may have been uplifted for a final time during the Laramide orogeny (Burberry et al., 2015) as the Laramide stress field is favorably oriented for transpressional movement with respect to many basement structures in the midcontinent (Tikoff & Maxson, 2001; Ohlmacher & Berendsen, 2005). Historic earthquakes have occurred in the study area, notably related to the southern boundary of the MRS and the eastern boundary of the NU (Ohlmacher & Berendsen, 2005), indicating that stress directions are still favorable for fault reactivation. However, overall, the region is considered to have been essentially tectonically quiescent since the Eocene, despite minor seismicity along structures such as the Nemaha anticline (Steeples et al., 1979).

Figure 3 indicates that there is no thick ductile unit in the study area, when the low ratio of shales to rigid units such as limestone and sandstone is taken into account (for a more detailed stratigraphy, refer to Condra & Reed (1959) and Jewett & Merriam (1959). Despite the units labeled as “interbedded x and shale”, the shale horizons have not acted as major decollement surfaces. The only documented fault activity is intraformational faulting (Neff, 1949; Merriam & Forster, 2002) and these authors do not describe large-scale detachment-style behavior. Thus, it is reasonable to assume (a) that the Paleozoic

sedimentary succession is behaving as a rigid beam and (b) that reactivation on deep-seated faults could have influenced the deformation of the entire rigid beam.

3. METHODS

The first phase of this study was carried out using a combination of remote sensing and field data collection. The remote dataset used was a series of Landsat Thematic Mapper images, obtained from NASA and processed under the MrSID algorithm (Tucker et al., 2004). This algorithm combines Band 7 (mid-infrared light) as red, Band 4 (near-infrared light) as green and Band 2 (visible green light) as blue. This produces a false color image in which bare rock surfaces are colored in shades of pink and brown (clastic units are darker than carbonate units) and vegetation appears in shades of green. Water typically appears dark blue-black (Figure 4). These images have a ground resolution of 28.5 m. Given that the study area is heavily vegetated, anomalies in the drainage network and variations in the vegetation patterns were used to interpret surface lineaments. Care was taken to avoid man-made irrigation systems (locally referred to as “waterways” by soil conservation personnel) and vegetation changes related to crop patterns; typically distinguishable from natural variation by scale and geometry. Man-made irrigation systems are generally smoothly curving, continuous with, or at right angles to, the pattern of terraces in the field, and confined to individual fields or sections. Vegetation changes related to crop patterns are typically oriented N-S or E-W in the study area and are typically perfectly straight lines. In contrast, natural drainage systems display patterns of tributaries, run for long distances and are related in some fashion to the underlying geology. Unexpected drainage geometries, such as straight segments with no evidence of man-made alteration, or sharp bends in a system were marked and used to guide the interpretation of lineaments.

Fracture data was collected at thirteen field sites, seven in SE Nebraska and six in NE Kansas, forming two transects across the study area. Transect 1 is made up from sites NF 1-NF 7 and is oriented E-W. Transect 2 is made up from sites KF 1-KF 6 and is oriented NE-SW. These data were collected in part because of limited outcrop availability and in part to have transects running broadly perpendicular to the anticipated trends of the main basement features. Bedding orientation data as well as fracture strike and dip was measured at each location. Outcrops were frequently road cuts, thus some bias is introduced into the data by the orientation of the road cut – for example, on an E-W oriented road cut, any fractures oriented E-W will be under-represented. This cannot be avoided, but was carefully noted for use in analysis. At

each site, 25 fracture orientations were measured. Care was taken to avoid radial fractures caused by dynamiting the outcrop in the road-construction process.

To gain a sense on the orientation of basement structures, we mapped lineaments using spatial analysis of gravity and magnetic grids (Bankey et al., 2002, Kucks, 1999). The magnetic anomaly grid was extracted from the North American Magnetic Anomaly Map database, comprising a compilation from numerous vintage airborne surveys that were leveled to a consistent elevation of 305 m above the terrain. In our study area, the flight line spacing varied from 0.5 – 8 km (Bankey et al. 2002). The total magnetic intensity data were reduced to magnetic pole in order to remove the skewness of magnetic signals due to non-verticality of the ambient field (inclination of 69.65°, a declination of 9.46°).

The gravity anomaly grid from Kucks, 1999 was used for the study. This dataset compiles the numerous land gravity measurements by the US Geological Survey, corrected for the rocks above sea level with an assumed density of 2.67 g/cc (Bouguer gravity anomaly). In order to remove the long-wavelength crustal signal from the gravity data, we generated the regional trend via upward continuation of observed gravity grid to a 100 km elevation. By removing this regional trend from the observed Bouguer gravity, we obtained the map of the residual Bouguer gravity anomalies, which represent the gravitational signal due to lateral density distribution in the subsurface rocks.

To further highlight the subsurface structures, we applied tilt derivative filters (Verduzo et al., 2004) to both the reduced to pole magnetic map and the residual Bouguer gravity grid. This procedure highlights the zones of the subtle changes in the potential fields in both vertical and horizontal directions. In gravity, an additional 5-km wide low-pass filter was necessary in order to remove some original gridding artifacts. The resultant filtered gravity and magnetic fields (Figure 5 a, b) show multiple lineaments associated with subsurface structures. The joint interpretation of the lineaments in both potential fields resulted in a map of potential faults in the basement rock.

4. RESULTS: SURFACE LINEAMENT/FRACTURE DATA

8,255 surface lineaments were mapped in the study area using Landsat images as described above, and the orientation of each lineament was calculated as a bearing. Only a subset of the main area is shown for ease of viewing (Figure 6). Lineaments visible in Figure 5 are predominantly oriented NE-SW. When all lineaments from the study area are displayed on a rose diagram (Figure 7), three prominent orientations can be noted (arrowed in Figure 7) – at 005, 055 and 085. About 8% of the data follows the 055 orientation,

forming the most significant orientation in the study area. Secondary peaks at 115 and 145 can also be noted in Figure 7 (not arrowed) although these orientations are only just above the apparent background or uniform distribution.

Figures 8-11 illustrate the data collected at each field site, after minor rotations were made to the dataset due to bedding dip. Figure 8 shows pole figures from the E-W oriented transect, NF 1-NF 7 and Figure 9 shows rose diagrams for the same data. Site NF 1 is in the Dakota Formation, at a highly weathered outcrop including numerous iron concretions south of Fairbury, NE. The sandstone at this outcrop is friable, but has fractured cleanly with a fracture spacing of about 1 m. There are three main fracture orientations, 057, 088 and 110, shown clearly by the clusters on the pole figure. No abutting relationships were discernable at this outcrop. Site NF2 is a blocky, systematically fractured outcrop of the Dakota Sandstone, south of NF 1. There are two prominent clusters on the pole figure, one of which can be separated into three orientations. These four orientations are 016, 040, 053 and 125. NF 3 is an outcrop of the Permian Wolfcampian series at a waterfall on private land. A thin, fractured limestone layer overlies a reddish shale unit. The pole figure appears to be a combination of both of the previous two, with fracture orientations prominently at 002, 031, 047, 090 and 122. NF 4 is a thinly bedded, highly fractured outcrop with chert nodules, along Plum Road between Liberty, NE and Wymore, NE. The units come from the Permian Wolfcampian Series (Figure 1). Prominent fracture orientations in this outcrop are at 029, 072 and 117. Site NF 5 is in the Virgilian Series of the Upper Pennsylvanian (Figure 1, Figure 3). The outcrop is a road cut along Highway 4, west of Table Rock, NE. A 1.5 ft thick layer of fossiliferous limestone is present, overlying thinly bedded limestone and shale. Bedding planes contain fossil hash, including spiriferids, other brachiopods, fenestrate bryozoan fragments, and crinoid ossicles. Prominent fracture orientations are 004, 026, 049, 068, 096 and 115. Site NF 6 is in the Virgilian Series of the Upper Pennsylvanian (Figure 1, Figure 3). The outcrop consists of a ridge of black shale overlain by a blocky recrystallized limestone containing crinoid fragments, thereby placing the outcrop close to the highstand of one of the Upper Pennsylvanian cyclothems. The outcrop is a quarry face within a succession of limestone and shale that is 18 ft thick and forms part of a fault scarp (Andy Keller, Martin Marietta Plant Manager, pers. comm.). The prominent fracture orientations are 034, 090, 105, 135 and 173. Lastly, site NF 7 is located close to a substation west of Humboldt, NE. The outcrop is a 1-ft thick layer of carbonate mudstone which is systematically fractured into blocks. The outcrop is considered to overly the Humboldt Fault (R.M. Joeckel, pers. comm.). Prominent fracture orientations are 019, 062, 073 and 173.

Figures 10 and 11 show pole figures and rose diagrams for field sites located along the NW-SE oriented transect in Kansas (KF 1-KF 6 respectively). Site KF 1 is an E-W oriented road cut exposing about 3 m of the Dakota Group. In this location, the Dakota Formation is manifest as a deep orange, cross-bedded sandstone, with evidence of re-precipitated or concentrated iron in bedding planes and cross-bedding. Prominent fracture sets are oriented 003, 022, 060, 084, 117 and 139. Site KF 2 is an outcrop of the Greenhorn Formation near Cuba, KS; a thinly bedded limestone and shale road cut containing inoceramids and oriented E-W. At this location, prominent fracture orientations are 008, 037, 111, 136 and 165. Site KF 3 is an outcrop of cherty, thickly-bedded limestone within the Wolfcampian Series of the Permian. The road cut is oriented N-S and is systematically fractured. Prominent fracture orientations at this outcrop are 359, 029, 068, 090, 110 and 137. Site KF 4 is also within the Permian Wolfcampian Series, and is a thinly-bedded, cherty limestone. The site is located close to the Fancy Creek State Park area of Tuttle Creek Lake. Prominent fracture orientations are 357, 029, 049, 072, 106, and 148. This is the only outcrop that shows the 148 orientation. Site KF 5 is within the Permian Wolfcampian Series and is a weathered outcrop close to the Tuttle Creek Spillway and the Spillway Fault System. Prominent fracture orientations here are 003, 021, 060, 072, 137 and 162. Lastly, site KF 6 is located south of Manhattan, KS, near the Konza Prairie Kansas Valley lookout point. The road cut is oriented N-S and is made up of interbedded limestone and shale from the Permian Wolfcampian Series. Prominent fracture orientations are 359, 020, 045, 078, 100 and 161.

Table 1 summarizes the pronounced fracture orientations at each outcrop, with the ETM (remote sensing) dataset included for comparison. The “mean” row in the table records the average orientation of each set of fractures, based on information in the table. The bolded numbers represent fracture sets appearing in both the field and remote datasets. The 001, 059, 090 and 110 orientations are found in both the ETM dataset and in 5 or more of the field sites. The 148 orientation is only found in one field site, but is prominent in the ETM dataset. Closer inspection of the table reveals that there is a subtle spatial trend appearing in the dataset, namely that orientations 137 and 163 only appear in the southern part of the study area (southern part of transect NF and the KF transect). However, neither of these trends are apparent in the ETM dataset.

Considering the data by age is also instructive. Figure 12 shows rose diagrams and pole figures for the Cretaceous, Permian and Pennsylvanian units, respectively, and Table 2 shows a summary of major fracture orientations. Note that the number of fractures in each plot is significantly different as there are more outcrops in the Permian units than in either Cretaceous or Pennsylvanian. Considering the dataset

by age shows that the 001 orientation appears in all datasets, as does the 090. Some important orientations, e.g. the 031 and 072 orientations only appear in the older units. Similarly, some orientations, such as the 124 and 163 orientations, are only prominent in the Permian and younger units. Finally, in this presentation of the data, orientations such as the 020, 046 and 059 only appear in the youngest (that is, the Cretaceous age) units.

5. RESULTS: BASEMENT LINEAMENTS FROM POTENTIAL FIELDS DATA

In the study area, 47 lineaments were mapped through a joint analysis of the filtered magnetic and gravity maps (Figure 13). Many of the lineaments correlate well with previously mapped basement faults (Figure 2). The interpreted lineaments show a strong NE-SW trend that mirrors the orientation of the MRS. This trend can clearly be seen when the plotted on a rose diagram (Figure 14). The majority of the lineaments (36%) are oriented at 025 and 045. In addition to the MCR parallel orientations, a strong NW-SE trend at 125 is also apparent with a smaller spike in the 145 direction.

6. COMPARISON OF SURFACE AND BASEMENT DATASETS

The basement lineaments in Figure 14 show the most tightly clustered orientations, when compared to Figures 7, 9, 11 and 12 (all other rose diagrams). The two prominent basement trends neatly mirror the CPO and MRS system faults known from other work (Figure 2). The CPO trend is not as strongly observed in the study area as is the MRS trend. Table 3 shows that all basement orientations appear in the surface dataset, and the overall NE-SW orientation appears in all three datasets, at either ~045 or ~055. This indicates that the surface datasets, both fracture and ETM-derived, are picking up the basement features but with varying amounts of dispersion. Figure 15 shows that there are areas (e.g. arrowed, marked S) where the ETM dataset is picking up the same orientation as the basement feature, and that there are areas (e.g. the region marked R) where the ETM dataset appears to be showing Riedel shears to the main basement lineament, as well as a similar orientation. Comparison of Figure 15 to Figures 8 and 9 (NF 3) shows that the main NE-SW ETM trend is on-trend with a basement lineament, but is a more minor trend in the measured fractures at this site. Overall, the surface fracture trends and the basement lineaments line up nicely, but the ETM dataset introduces a significant amount of noise into the system. This correspondence of lineament and fracture orientations is best explained by repeated reactivation on the basement faults, as detailed in the “Geological Setting” section, throughout the Pennsylvanian, Permian

(both ARM-related) and lower Cretaceous. A Cretaceous phase of reactivation is less well documented than the other ARM-related reactivation, and could be due to far-field stresses from the Laramide Orogeny.

7. DISCUSSION

As noted above, the basement lineaments (Figures 13, 14) mirror the trends of Precambrian age faults related to the MRS and the CPO. Overall, the correspondence of surface lineaments and fractures to basement data indicates reactivation of basement structures in an important influencing factor in the development of the surface features in Nebraska and Kansas. Our results enhance the work of Neff (1949), Nelson (1952), Baehr (1954), Ward (1968), Smith et al. (1974) and White (1990) by extending the dataset of fractures and satellite-derived lineaments, and documenting the relationships with basement features over a wider area. We have further shown that the strong presence of the MRS-related basement orientation in the Cretaceous age datasets (Figures 12, 14) provides strong evidence for reactivation of the MRS trends in the mid Cretaceous.

The surface and ETM datasets are much more dispersed than the basement dataset. We first need to consider that the depth to the basement is significant in the study area, leading to attenuation of the gravity and magnetic signature of buried structures. As a result, only dominant subsurface features will be represented in the basement analysis, compared to a much wider range of features represented at the surface. One possibility for dispersion in surface datasets, alluded to above, is the generation of secondary fracture orientations during reactivation as strike slip faults. This can be seen in the development of fractures in Riedel shear orientations (Figure 15). Another possibility is that flexure and uplift of the rigid beam of Phanerozoic sediments is distributing deformation across a wider area, perhaps by outer-arc extension of the thick beam above a vertically uplifting basement feature. Lastly, fractures are known to develop in unroofing, that is, uplift and erosion, situations, although these are typically small-scale and more randomly oriented. Lineament analysis on this scale and at this resolution is unlikely to pick up many unroofing structures, but some of the noise in the field datasets (Figures 8-12) may be attributed to this. An additional factor that must be considered in the evaluation of Figure 12 is that sandstone layers typically fracture in a much blockier, systematic fashion than the underlying limestones. Limestone containing numerous fossil fragments appears to fracture with more dispersion around the key orientations than a sandstone layer of a similar thickness, subjected to the same stresses (see e.g.

Burberry & Peppers, 2017; Burberry et al., in review). This leads to more prominent trends in the Cretaceous rose diagram (Figure 12) than those observed in the Permian or Pennsylvanian diagrams.

The misfit between surface fracture data and ETM datasets has also been documented by other authors (e.g. McQuillan, 1974; Siddoway, 2011). These authors demonstrate that fracture networks generated by remote and field measurement are statistically different from one another, i.e. the mean resultant direction and standard deviation for each dataset is significantly different. McQuillan (1974), shows that the mean resultant fracture direction in an air-photo dataset from Kuh-e-Asmari, Iran, is not easily observable on the ground. A similar problem was noted in work on the Bighorn Mountains (Siddoway, 2011) where the dominant fracture directions are similar in remote and field datasets, but not identical. No explanation has been offered for this discrepancy (Siddoway, pers. comm.). The dataset presented in this study suffers from a similar mismatch between fracture and ETM data, likely because of the smoothing in the remote dataset over a series of structures and over two markedly different lithologies, , and the challenge of working with 30m resolution data. Nonetheless, we have documented the strong reactivation of the MRS in all three datasets.

8. CONCLUSIONS

We have documented lineaments and fractures across a series of different spatial scales in southeast Nebraska and northeast Kansas. The prominent basement orientations are NE-SW and NW-SE, which orientations are mirrored in the ETM and fracture datasets. Distributed strain throughout the Phanerozoic rigid beam that is uplifted over the basement features adds dispersion and secondary orientations to both the ETM and fracture dataset. The prominence of the NE-SW orientation in Cretaceous age rocks indicates a reactivation of MRS structures after the mid-Cretaceous, likely a result of far field stresses from the Laramide Orogeny. Lastly, this combined study shows the importance of subtle surface data in showing activity on deep-seated basement faults in the absence of large-scale structure development.

388 Table 1: Summary of fracture orientations for all field sites, organized by transect. The ETM data is given
389 for comparison

NF 1					057		088	110				
NF 2		016		040	053				125			
NF 3	002		031	047			090		122			
NF 4			029			072		117				
NF 5	004		026	049		068	096	115				
NF 6	353		034				090	105		135		
NF 7	353	019			062	073						
KF 1	003	022			060		084	117		139		
KF 2	008		037					111		136		165
KF 3	359		029			068	090	110		137		
KF 4	357		029	049		072		106			148	
KF 5	003	021			060	072				137		162
KF 6	359	020		045		078		100				161
Mean	***001***	*020*	*031*	*046*	***059***	*072*	***090***	***110***	*124*	*137*	***148***	*163*
ETM	005				055		085	115			145	

390

391

392 Table 2: Summary of main fracture orientations in field sites organized by age. The mean and ETM data
393 are given for comparison

All K	004	015		040	050		089	110	122			161
All Perm	003		029			074	098		118			159
All Penn	003		028			069	091	113		135		
Mean (Table 1)	***001***	*020*	*031*	*046*	***059***	*072*	***090***	***110***	*124*	*137*	***148***	*163*
ETM	005				055		085	115			145	

394

395

Table 3: Summary of key fracture orienrataions from each dataset. The mean orientations from surface fractures, orientations from ETM analysis and orientations from potential fields analysis are shown.

Basement		025		045					125	135		
Mean (Table 1)	001	020	031	046	059	072	090	110	124	137	148	163
ETM	005				055		085	115			145	

REFERENCES

Anderson, K.H. & Wells, J.S., 1968. Forest City Basin of Missouri, Kansas Nebraska and Iowa. AAPG Bulletin, 52 (2) p264-281

Atekwana, E., 1996. Precambrian basement beneath the central Midcontinent United States as interpreted from potential field imagery. GSA Special Paper 308, p33-44

Audet, P. & Burgmann, R., 2011. Dominant role of tectonic inheritance in supercontinent cycles. Nature Geoscience 4, 184–187 doi:10.1038/ngeo1080

Baars, D.L., 1992. Conjugate basement rift zones in Kansas, Midcontinent, USA. *In* Rickard, M.J., Harrington, H.J. & Williams, P.R. (eds) Basement Tectonics 9, Australia and Other Regions, Proceedings of the International Conferences on Basement Tectonics v5, p201-210.

Bahroudi, A. & Koyi, H.A., 2003. Effect of spatial distribution of Hormuz salt on deformation style in the Zagros fold and thrust belt: an analogue modelling approach. Journal of the Geological Society, 160, p719-733

Baehr, W.M., 1954. An investigation of the relationship between rock structure and drainage in the southern half of the Junction City, Kansas, quadrangle. Unpubl. MS thesis, Kansas State College of Agriculture and Applied Science.

Bankey, V., Cuevas, A., Daniels, D., Finn, C. A., Hernandez, I., Hill, P., Kucks, R., Miles, W., Pilkington, M., Roberts, C., Roest, W., Rystrom, V., Shearer, S., Snyder, S., Sweeney, R., Velez, J., Phillips, J.D., and Ravat, D., 2002, Digital data grids for the magnetic anomaly map of North America: U.S. Geological Survey Open-File Report 02-414, U.S. Geological Survey, Denver, Colorado, USA, https://mrdata.usgs.gov/magnetic/

Berendsen, P., Doveton, J. H., & Speczik, S., 1992. Distribution and characteristics of a Middle Ordovician oolitic ironstone in northeastern Kansas based on petrographic and petrophysical properties: a Laurasian ironstone case study. *Sedimentary geology*, v. *76*(3-4), p. 207-219.

Berendsen, P., 1997. Tectonic evolution of the Midcontinent Rift System in Kansas. GSA Special Paper 312, p235-241

Berendsen, P., & Speczik, S. (1991). Sedimentary environment of Middle Ordovician iron oolites in northeastern Kansas, USA. *Acta Geologica Polonica*, v. *41*(3-4), p. 215-226.

Brown, L., Serpa, L., Setzer, T., Oliver, J., Kaufman, S., Lillie, R., Steiner, D. & Steeples, D.W., 1983. Intracrustal complexity in the United States midcontinent: Preliminary results from COCORP surveys in northeastern Kansas. Geology 11 p25-30

Burberry, C.M., 2015. The effect of basement fault reactivation on the Triassic-Recent geology of Kurdistan, N Iraq. Journal of Petroleum Geology, v38 (1) p37-58

Burberry, C.M. & Peppers, M.H., 2017. Fracture Characterization in Tight Carbonates: an example from the Ozark Plateau, AR. AAPG Bulletin, v. 101, p. 1675-1696

435 Burberry, C.M., Cannon, D.L., Cosgrove, J.W. & Engelder, T., Fracture patterns associated with the
436 evolution of the Teton anticline, Sawtooth Range, Montana. In review for Geological Society of London
437 Special Publication

438 Butler RWH., Holdsworth, R.E & Lloyd, G.E. 1997. The role of basement reactivation in continental
439 deformation. Journal of the Geological Society, v154, p69-71. Doi: 10.1144/gsjgs.154.1.0069

440 Butler, R. W. H., Tavarnelli, E. & Grasso, M. 2006. Structural inheritance in mountain belts: An Alpine
441 Apennine perspective. Journal of Structural Geology 28, 1893-1908.

442 Carlson, M., 1995. Tectonic implications and influence of the midcontinent rift system in Nebraska and
443 adjoining areas. *In* Ojakangas, R.W., Dickas, A.B. & Green, J.C. (eds) Basement Tectonics 10, Proceedings
444 of the International Conferences on Basement Tectonics v4, p61-64.

445 Carlson, M.P., 1997. Tectonic implications and influence of the Midcontinent Rift System in Nebraska
446 and adjoining areas. GSA Special paper 312, p231-234

447 Carlson, M., 1998. Evidence from the stratigraphic record for basement deformation in southeastern
448 Nebraska, Midcontinent USA. *In* Hogan, J.P & Gilbert, M.C. (eds) Basement Tectonics 12, Central North
449 America and Other Regions, Proceedings of the International Conferences on Basement Tectonics v6,
450 p227.

451 Carlson, M.P., 2007. Precambrian accretionary history and Phanerozoic structures – a unified
452 explanation for the tectonic architecture of the Nebraska region, USA. GSA Memoir 200, p321-326

453 Carlson, M.P. & Treves, S., 2005. The Elk Creek carbonatite, southeast Nebraska – an overview. Natural
454 Resources Research, 14 (1) p39-45

455 Cinque, A., Patacca, E., Scandone, P., & Tozzi, M. (1993). Quaternary kinematic evolution of the Southern
456 Appennines. Relationships between surface geological features and deep lithospheric structures. Annals
457 of Geophysics, v. 36, p. 249-260.

458 Condra, G.E. & Reed, E.C., 1959. The Geological Section of Nebraska. Nebraska Geological Survey Bulletin
459 14A, 82pp

460 Craddock, J.P., Pearson, A., McGovern, M., Kropf, E., Moshoian, A. & Donnelly, K., 1997. Post-extension
461 shortening strains preserved in calcites of the Midcontinent Rift. GSA Special paper 312, p115-126

462 Del Ventisette, C., Montanari, D., Sani, F. & Bonini, M. 2006. Basin inversion and fault reactivation in
463 laboratory experiments. Journal of Structural Geology 28, 2067-2083.

464 Dewey, J. F. 1989. Kinematics and Dynamics of basin inversion. In: Geological Society of London Special
465 Publication (edited by Cooper, M. A. & Williams, W. D.) 44, 352.

466 Eardley, A.J., 1962. Structural geology of North America. Harper & Row, New York, 743pp

467 Gates, A.E. & Costa, R.E. 1998. Multiple Reactivation of Rigid Basement block margins, examples in the
468 northern Reading Prong, USA. *In* Hogan, J.P & Gilbert, M.C. (eds) Basement Tectonics 12, Central North
469 America and Other Regions, Proceedings of the International Conferences on Basement Tectonics v6,
470 p123 -153.

Gay, S. P. Jr., 1999. Strike-slip compressional thrust-fold nature of the Nemaha System in Eastern Kansas and Oklahoma. Transactions of the 1999 AAPG Midcontinent section meeting, p39-50

Goebel, E. D. (1968). Mississippian rocks of western Kansas. *AAPG Bulletin*, v. *52*(9), p. 1732-1778.

Hauser, E.C., 1996. Midcontinent rifting in a Grenville Embrace. GSA Special Publication 308, p67-75

Heckel, P. H. (2008). Pennsylvanian cyclothems in Midcontinent North America as far-field effects of waxing and waning of Gondwana ice sheets. *Resolving the Late Paleozoic Ice Age in Time and Space; Fielding, CR, Frank, TD, Isbell, JL, Eds*, 275-29

Heckel, P. H., 2013. Pennsylvanian stratigraphy of Northern Midcontinent Shelf and biostratigraphic correlation of cyclothems. *Stratigraphy*, v. *10*, p. 3-39

Huerta, A.D. & Harry, D.L. 2012. Wilson cycles, tectonic inheritance, and rifting of the North American Gulf of Mexico continental margin. Geosphere, April 2012, v. 8, p. 374-385

Joeckel, R. M., Nicklen, B. L., & Carlson, M. P. (2007). Low-accommodation detrital apron alongside a basement uplift, Pennsylvanian of Midcontinent North America. Sedimentary Geology, v. 197(1-2), p. 165-187.

Kluth, C.F. & Koney, P.J., 1981. Plate tectonics of the Ancestral Rocky Mountains. Geology 9, p10-15.

Kucks, R.P., 1999. Bouguer gravity anomaly data grid for the conterminous US, U.S. Geological Survey, https://mrdata.usgs.gov/gravity/

Macedo, J. & Marshak, S., 1999. Controls on the geometry of fold-thrust belt salients. GSA Bulletin, 111 (12), p1808-1822

McClay, K.R., 1995. The geometries and kinematics of inverted fault systems: a review of analogue model studies. Geological Society of London Special Publication 88, p97-118.

McMechan, M.E. 2012. Deep transverse basement structural control of mineral systems in the southeastern Canadian Cordillera. Canadian Journal of Earth Sciences, 2012, 49(5): 693-708, 10.1139/e2012-013

McQuillan, H., 1974. Fracture Patterns on Kuh-e Asmari Anticline, SW Iran. AAPG Bulletin, v58 (2) p236-245

Mendenhall, R.A., 1958. Surface Geology of Bala, Riley County, Kansas. Unpubl. MS thesis, Kansas State College of Agriculture and Applied Science.

Molliex, S., Bellier, O., Terrier, M., Lamarche, J., Martelet, G. & Espurta, N. 2010. Tectonic and sedimentary inheritance on the structural framework of Provence (SE France): Importance of the Salon-Cavaillon fault. Tectonophysics, 501, p1-16

Moore, R.C., 1926. Early Pennsylvanian deposits west of the Nemaha Granite Ridge, Kansas. AAPG Bulletin 10 (3) p205-216

Neff, A.W., 1949. A study of the fracture patterns of Riley County, Kansas. Unpubl. MS thesis, Kansas State College of Agriculture and Applied Science.

Nelson, P.D., 1952. The reflection of the basement complex in the surface structures of the Marshall-Riley county area of Kansas. Unpubl. MS thesis, Kansas State College of Agriculture and Applied Science.

Obaid A.K., & Allen, M.B., 2017. Landscape maturity, fold growth sequence and structural style in the Kirkuk Embayment of the Zagros, northern Iraq. Tectonophysics, v. 717, p. 27-40

Ohlmacher, G.C. & Berendsen, P. 2005. Kinematics, mechanics, and potential earthquake hazards for faults in Pottawatomie County, Kansas. USA. Tectonophysics 396, p227-244.

Osmundsen, P.T., Henderson, I.,Lauknes, T.R., Larsen, Y., Redfield, T.F. & Dehls, J., 2009. Active normal fault control on landscape and rock-slope failure in northern Norway. Geology ; 37 (2): 135–138. doi: https://doi.org/10.1130/G25208A.1

Ranalli, G., 2000. Rheology of the crust and its role in tectonic reactivation. Journal of Geodynamics, 30, p3-15

Said, A., Baby, P., Chardon, D. & Ouali, J. 2011. Structure, paleogeographic inheritance, and deformation history of the southern Atlas foreland fold and thrust belt of Tunisia. Tectonics, 30. doi:10.1029/2011TC002862

Scotese, C. R., & Golonka, J. (1992). PALEOMAP paleogeographic atlas: Arlington. University of Texas, Department of Geology, PALEOMAP Progress Report, 20.

Serpa, L., Setzer, T. & Brown, L., 1989. COCORP seismic-reflection profiling in northeastern Kansas, In Steeples, D,W, (ed) Geophysics in Kansas: Kansas Geological Survey, Bulletin 226, pp. 165-176

Sibson, R.H., 1985. A note on fault reactivation. Journal of Structural Geology 7 (6) p751-754

Siddoway, C., 2011. Potential sources of crustal anistotropy in the Wyoming province: insights from basement structures of the Bighorn mountains, Wyoming. GSA Abstracts with programs, vol 42 (5) p435

Smith, J.W., Kuntz, C.S., Williams, A.L. & Scheper, R.J., 1974. Structural and Photographic Lineaments, Gravity, Magnetics and Seismicity of Central USA. Proceedings of the First International Conference on the New Basement Tectonics, Pages 163-168

Steeples, D. W., DuBois, S. M., & Wilson, F. W. (1979). Seismicity, faulting, and geophysical anomalies in Nemaha County, Kansas: Relationship to regional structures. *Geology*, v. 7, p. 134-138.

Thomas, W. A. 2004. Genetic relationship of rift-stage crustal structure, terrane accretion, and foreland tectonics along the southern Appalachian-Ouachita orogen. Journal of Geodynamics 37(3-5), 549-563.

Tikoff, B; & Maxson, J., 2001. Lithopsheric buckling of the Laramide Foreland during Late Cretaceous and Paleogene, Western United States. Rocky Mountain Geology 36 (1) p13-35.

Tucker, C. J., D. M. Grant, and J. D. Dykstra, 2004. NASA's global orthorectified Landsat data set. Photogrammetric Engineering & Remote Sensing, V. 70, no. 3, p. 313–322.

Verduzco, B., Fairhead, J.D., Green, C.M., and MacKenzie, C., 2004, New insights into magnetic derivatives for structural mapping. The Leading Edge, v. 23, p. 116- 119.

Viola, G., Odonne, F. & Mancktelow, N., 2004. Analogue modelling of reverse fault reactivation in strike–slip and transpressive regimes: application to the Giudicarie fault system, Italian Eastern Alps. Journal of Structural Geology, 26 (3) p401-418.

Ward, J.R., 1968. A Study of the Joint Patterns in Gently Dipping Sedimentary Rocks of South-Central Kansas. Kansas Geological Survey Bulletin 191 pt 2.

White, D.C. 1990. Lineament study of stream patterns in a portion of east-central Kansas. Unpubl. MS Thesis, Emporia State University

Whitmeyer, S. J., & Karlstrom, K. E. (2007). Tectonic model for the Proterozoic growth of North America. Geosphere, 3(4), 220-259.

Williams, G. D., Powell, C. M. & Cooper, M. A. 1989. Geometry and kinematics of inversion tectonics. In: Inversion Tectonics (edited by Cooper, M. A. & Williams, G. D.). Geological Society of London Special Publication 44, 3-15.

Wilson, F.W. & Berendsen, P. The role of recurrent tectonics in the formation of the Nemaha uplift and Cherokee-forest city basins and adjacent structures in eastern Kansas and contiguous states, USA. *In* Hogan, J.P & Gilbert, M.C. (eds) Basement Tectonics 12, Central North America and Other Regions, Proceedings of the International Conferences on Basement Tectonics v6, p301-302.

Preprints (www.preprints.org) | NOT PEER-REVIEWED | Posted: 8 April 2018 doi:10.20944/preprints201804.0092.v1

Peer-reviewed version available at *Geosciences* **2018**, *8*, 215; doi:10.3390/geosciences8060215

571 Figures and Captions

572 Figure 1

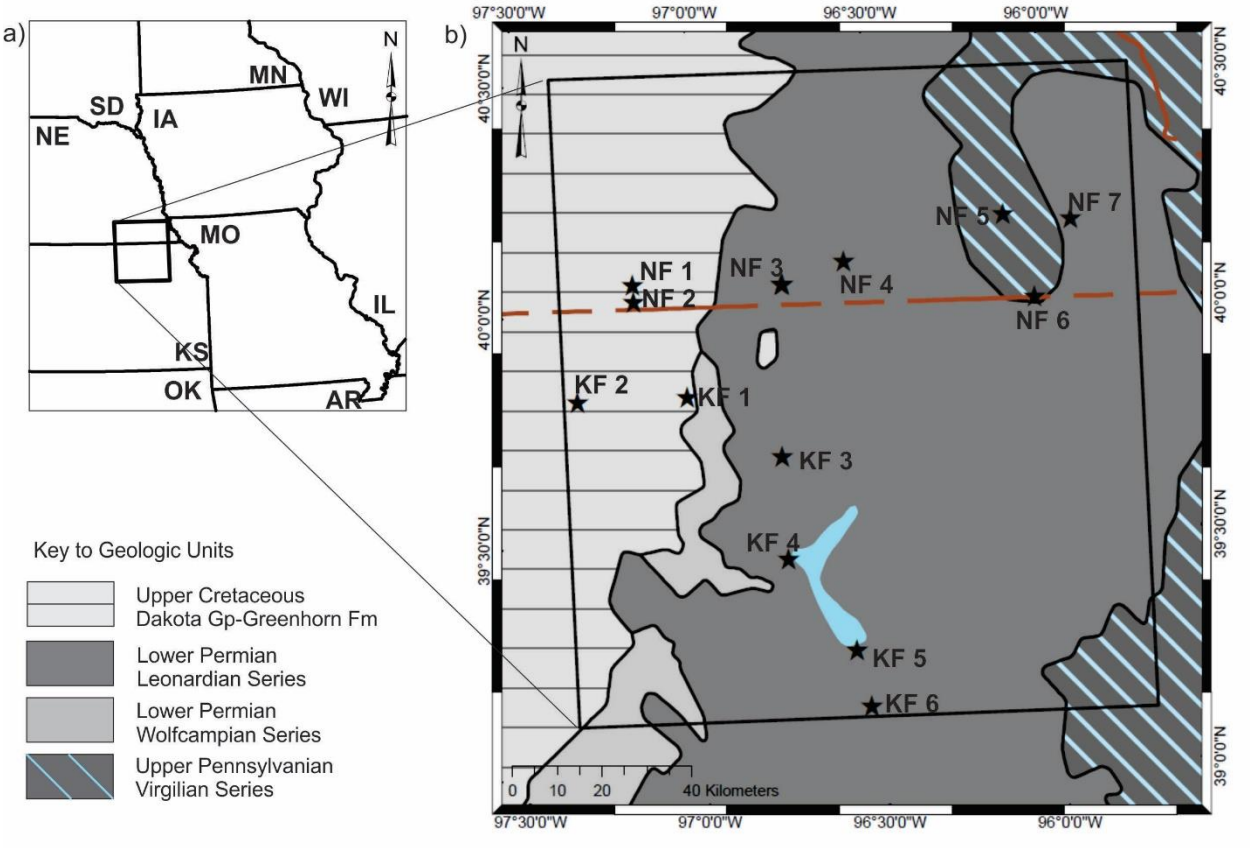

573

574 Figure 1: Simplified geologic map of southeastern Nebraska and northeastern Kansas, based on the
575 GDNA (REF). The study area is shown as a black box, and locations of field sites are shown as black dots.
576 The inset shows the location of the studied region within the conterminous US.

577

578

579

580

581

582

583

584

585

586

587 Figure 2

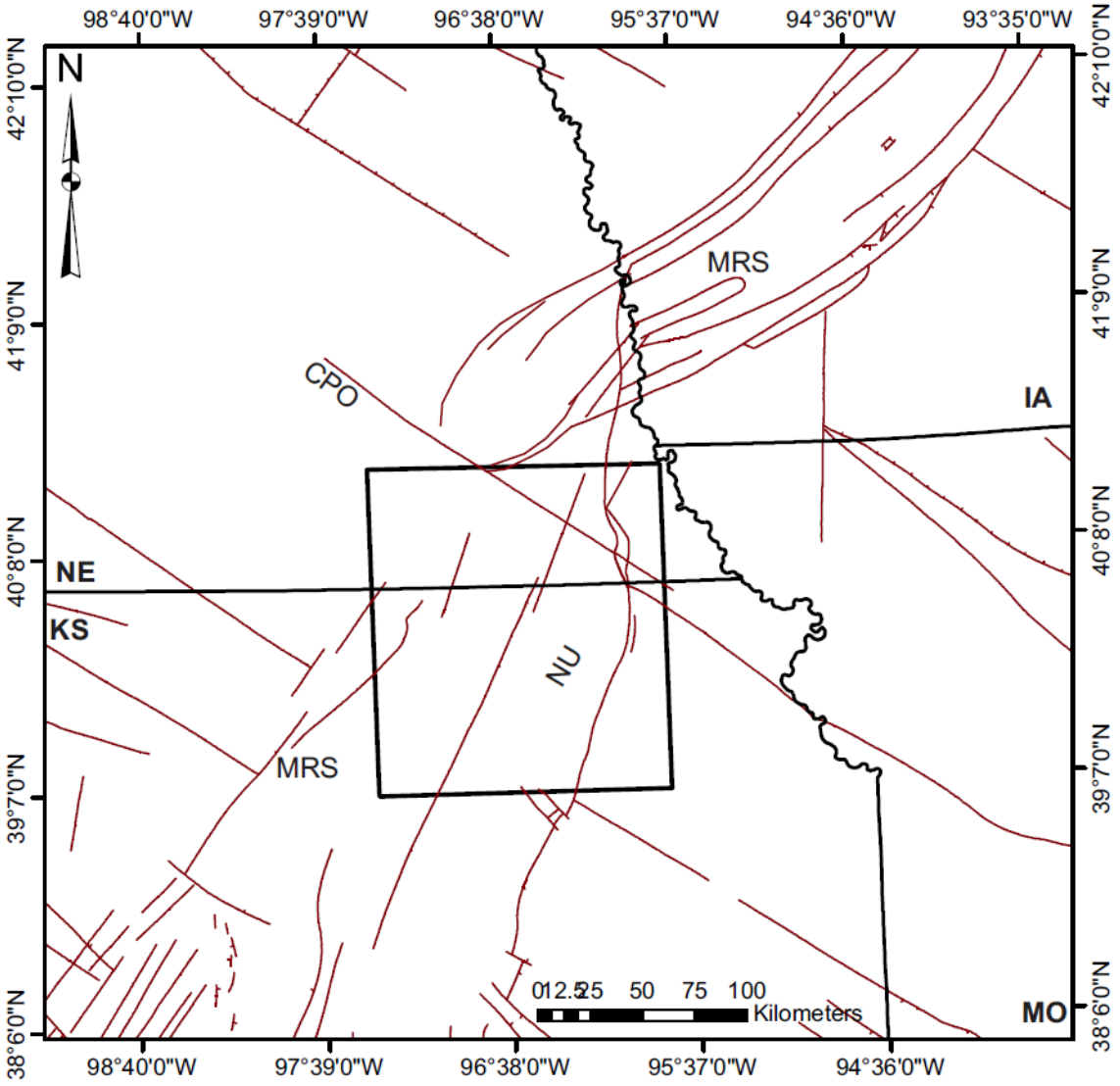

588

589 Figure 2: Existing map of basement faults in the study area and beyond, after Burbery et al., 2015. Key
590 features mentioned in the text are marked: MRS – Midcontinent Rift System, CPO – Central Plains
591 Orogen trend, NU – Nemaha Uplift.

592

593

594

595

596

597

Preprints (www.preprints.org) | NOT PEER-REVIEWED | Posted: 8 April 2018 doi:10.20944/preprints201804.0092.v1

Peer-reviewed version available at Geosciences 2018, 8, 215; doi:10.3390/geosciences8060215

598 Figure 3

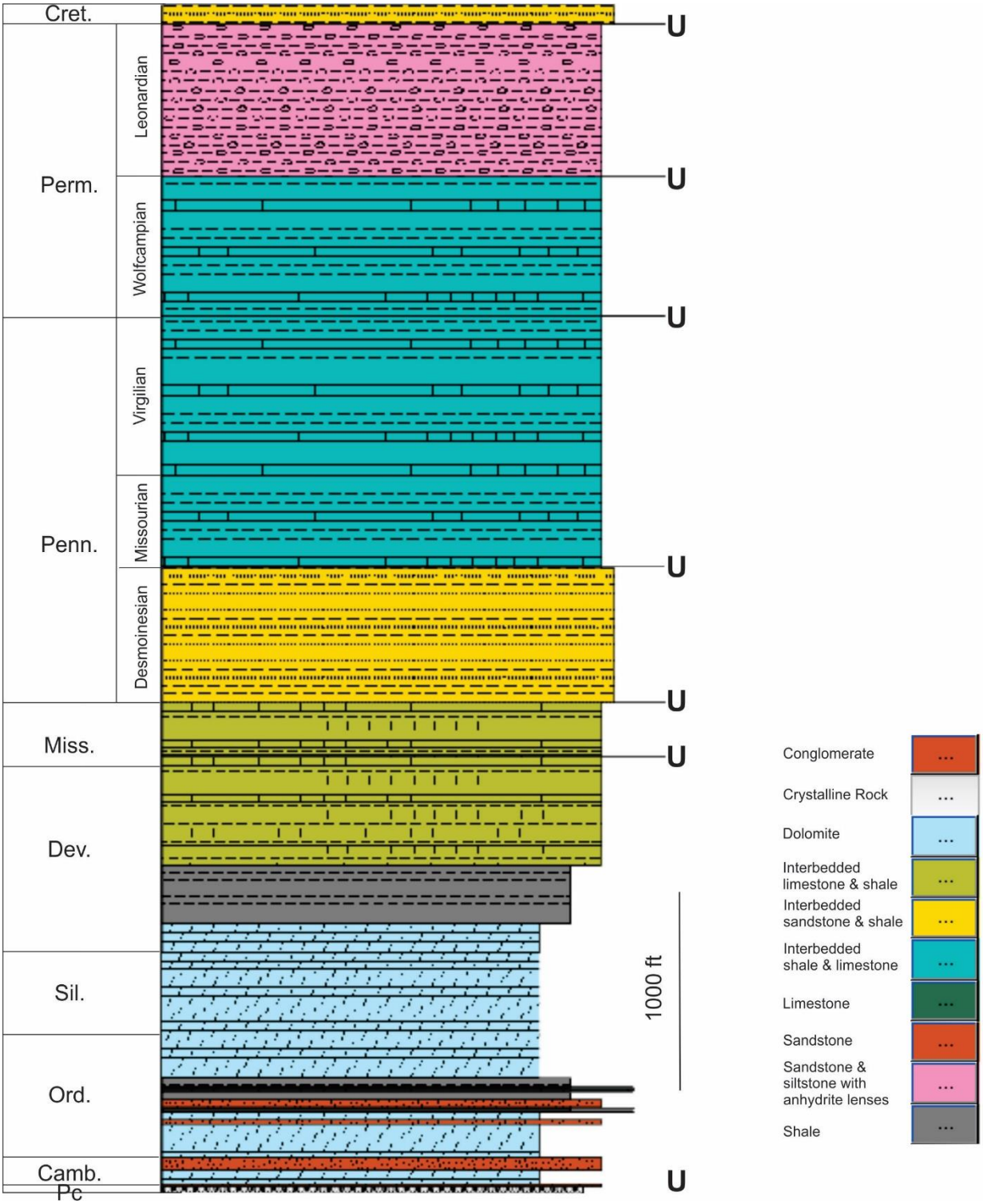

599

600 Figure 3: Composite, simplified stratigraphic column of the study area, with major unconformities
601 marked.

602

603

604 Figure 4

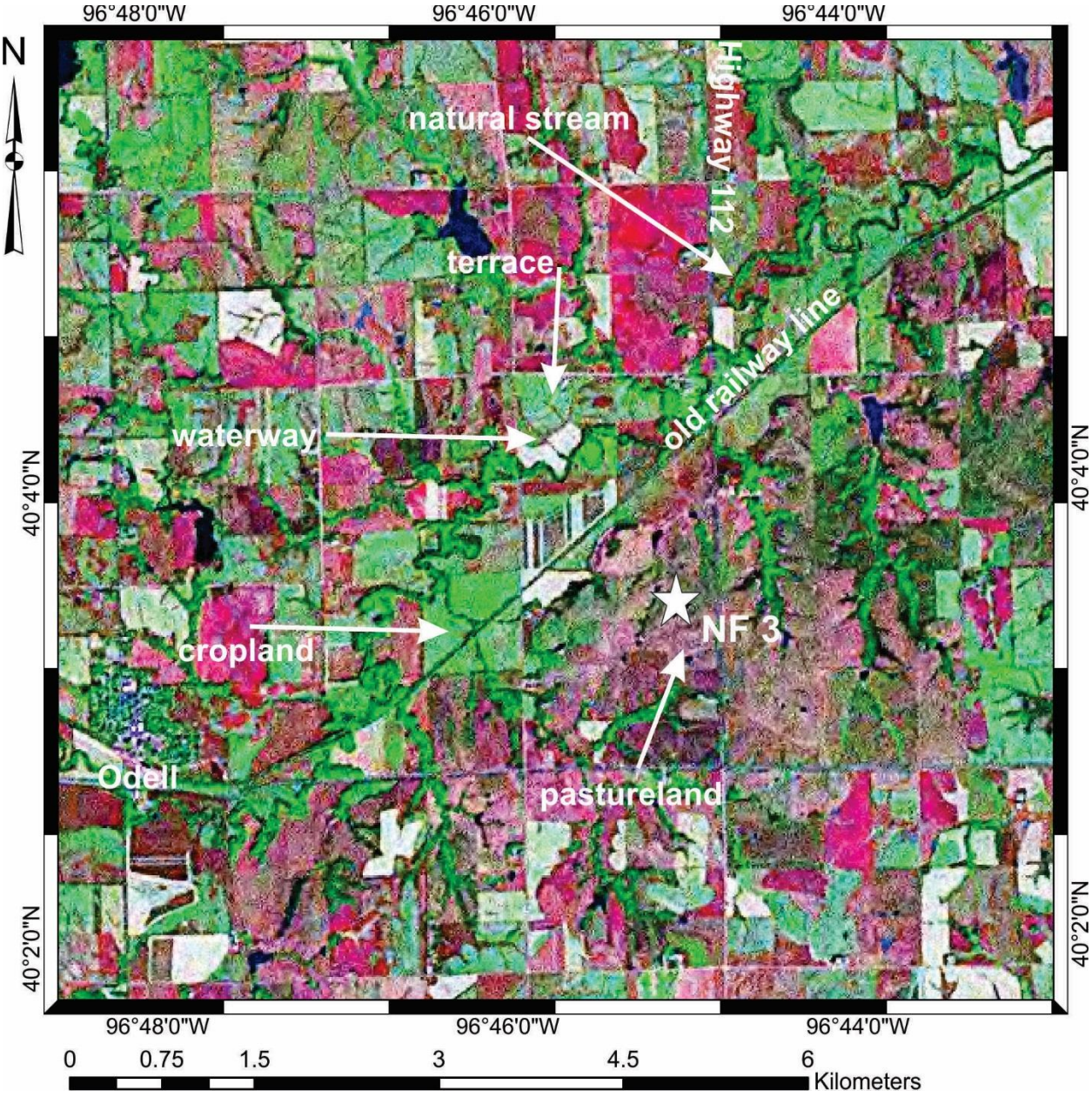

605

606 Figure 4: MrSID image, illustrating the general color balance in the area, the difference between
607 waterways and real rivers and the difference between crop-induced vegetation patterns and the
608 "natural" vegetation changes. The star marks the location of site NF 3.

609

610

611

612

613 Figure 5

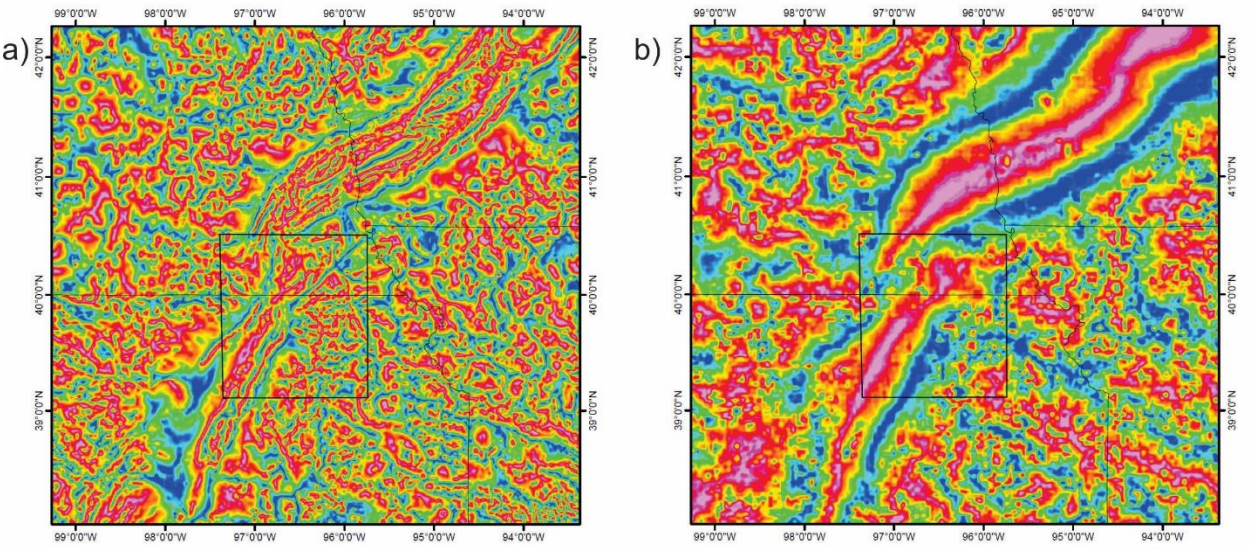

614

615 Figure 5: a) Reduced-to-the-pole magnetic map with tilt derivative applied and b) tilt derivative of the
616 residual bouguer gravity anomaly. The black box denotes the study area.

617

618

619

620

621

622

623

624

625

626

627

628

629

630

631

632

633 Figure 6

634

635 Figure 6: MrSID image from Figure 4, above, this time with lineaments marked in black. White star
636 represents the location of site NF 3.

637

638

639

640

641

642 Figure 7

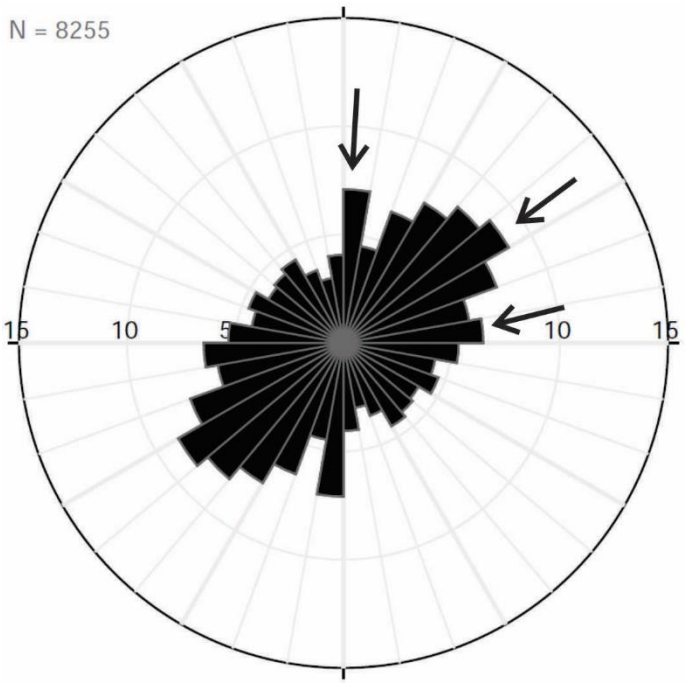

643

644 Figure 7: Rose diagram showing orientations of all lineaments picked from satellite data in the study
645 area. Each division on the rose diagram represents 10 degrees.

646

647 Figure 8

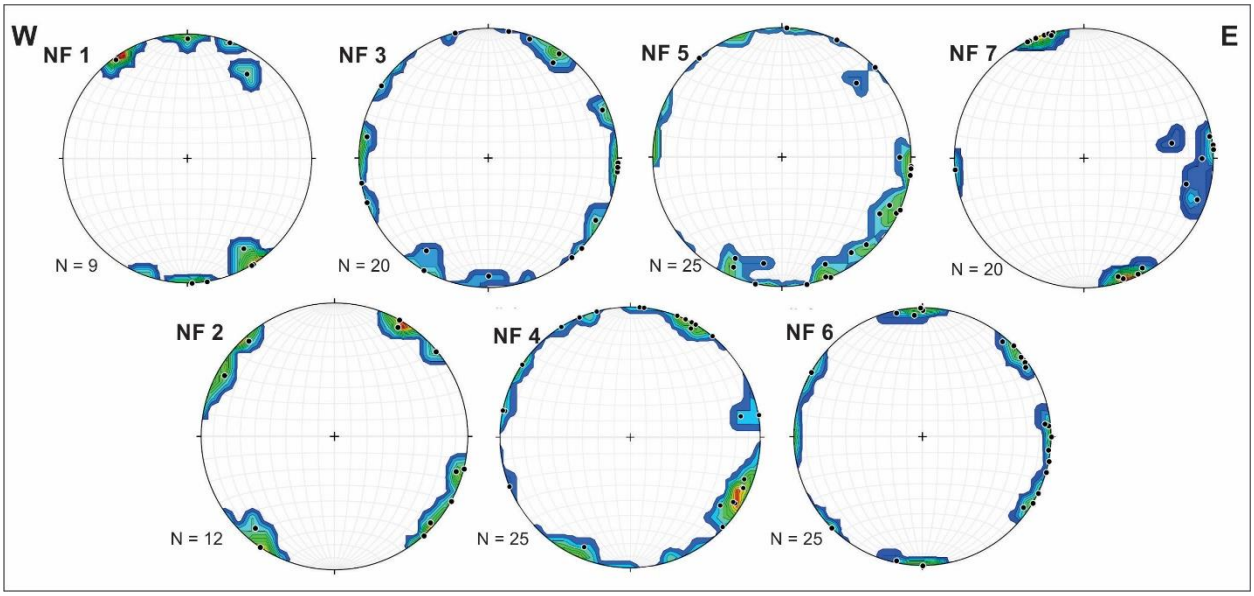

648

649 Figure 8: Contoured poles to planes for fractures at each site on the E-W transect. Sites are arranged in
650 order from W to E. The number of fractures in each figure is shown at the bottom left.

651

652 Figure 9

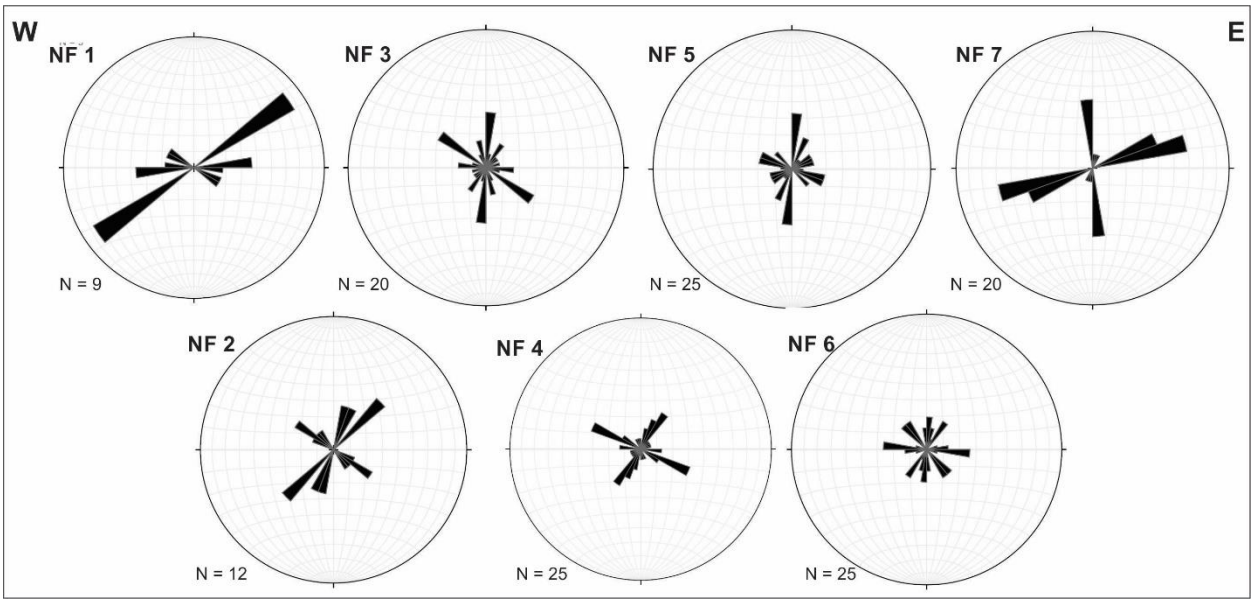

653

654 Figure 9: Rose diagrams for fractures at each site on the E-W transect. Sites are arranged in order from
655 W to E. The number of fractures in each figure is shown at the bottom left.

656

657

658 Figure 10

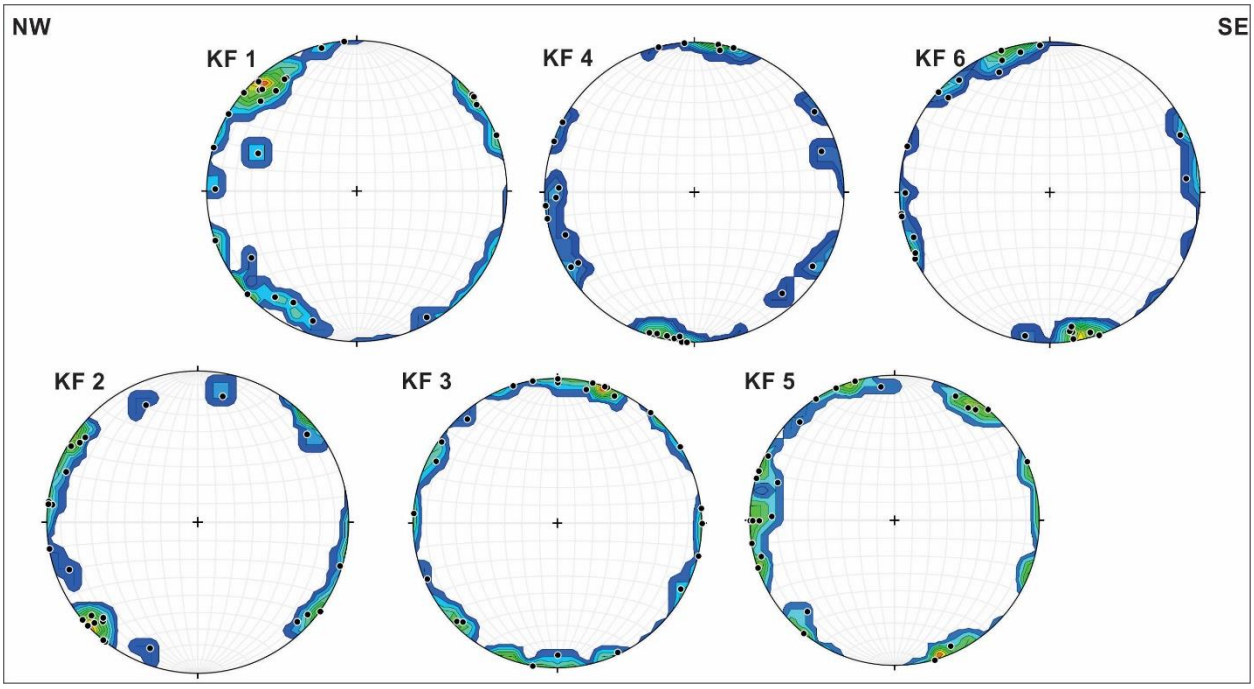

659

660 Figure 10: Contoured poles to planes for fractures at each site on the NW-SE transect. Sites are
661 arranged in order from NW to SE. Each figure represents 25 fractures.

662 Figure 11

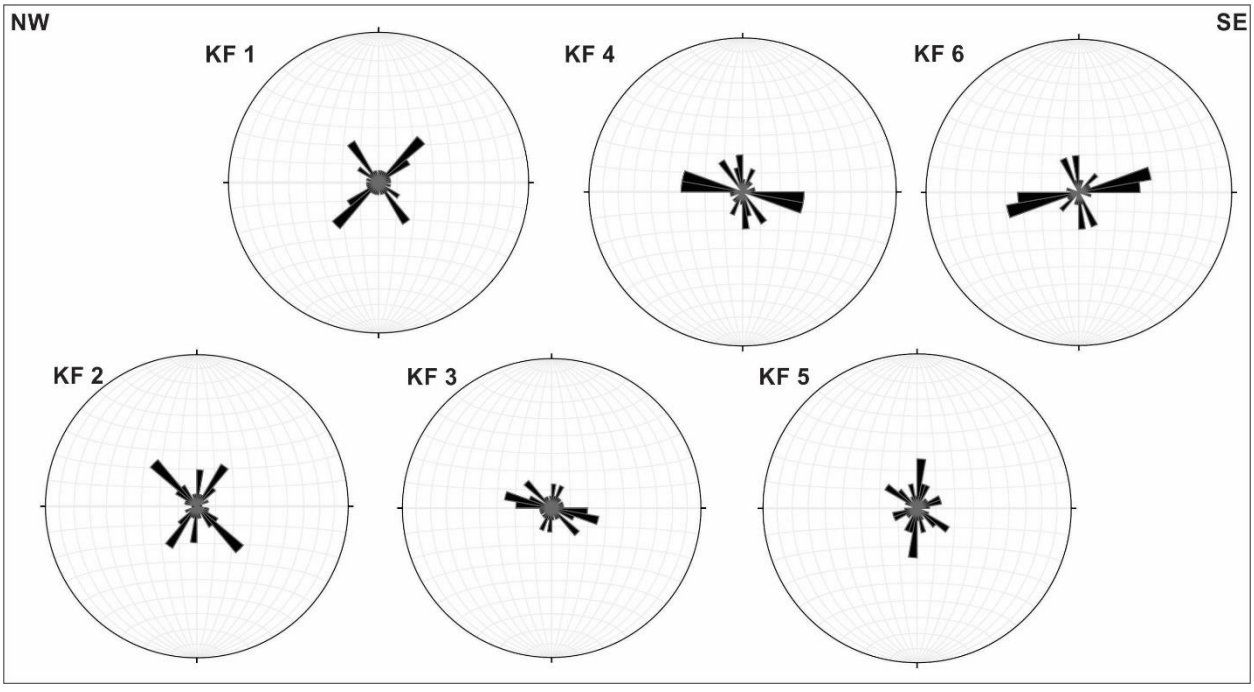

663

664 Figure 11: Rose diagrams for fractures at each site on the NW-SE transect. Sites are arranged in order
665 from NW to SE. Each figure represents 25 fractures

666 Figure 12

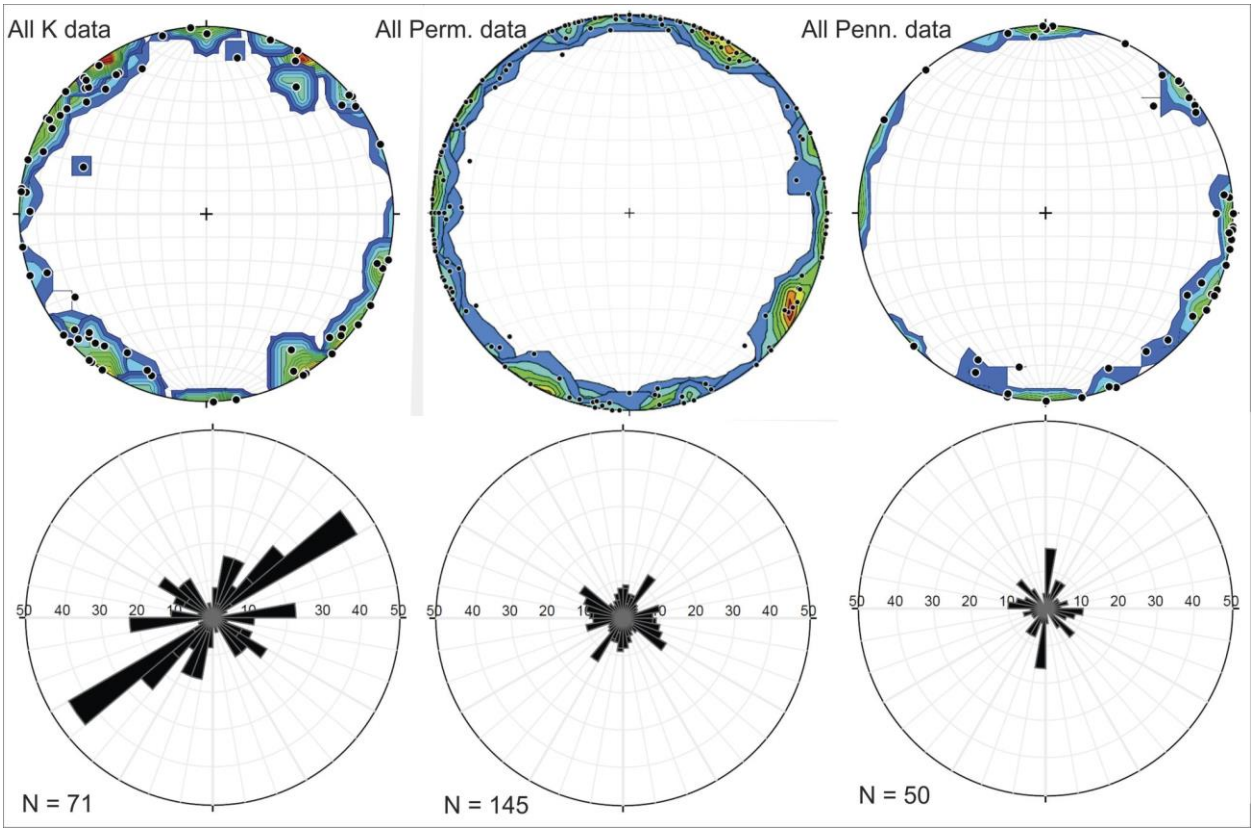

667

668 Figure 12: Contoured poles to planes and rose diagrams for the fracture data grouped by age instead of
669 separated by location.

670

671

Preprints (www.preprints.org) | NOT PEER-REVIEWED | Posted: 8 April 2018 doi:10.20944/preprints201804.0092.v1

Peer-reviewed version available at Geosciences 2018, 8, 215; doi:10.3390/geosciences8060215

672 Figure 13

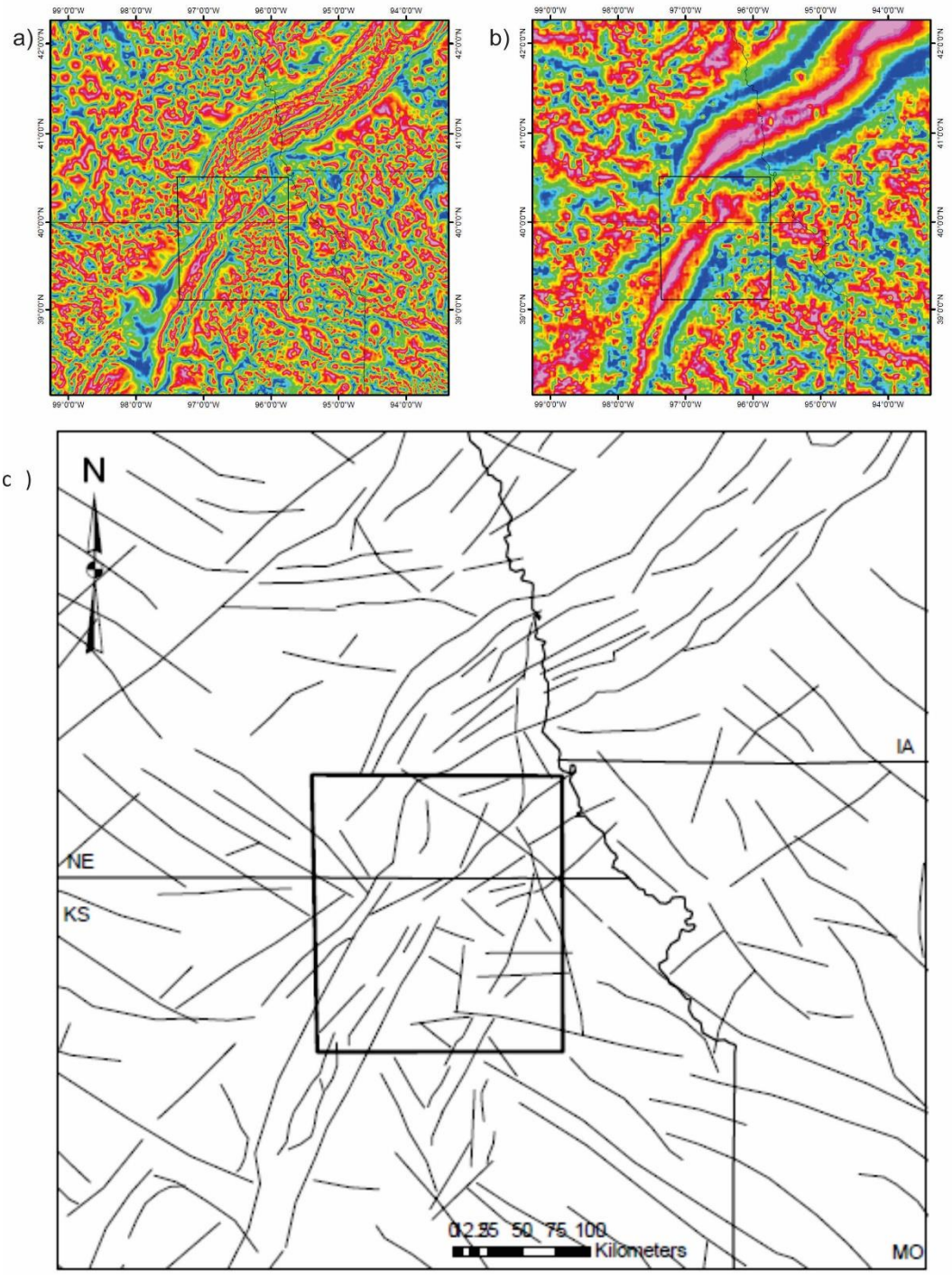

673

674 Figure 13: Lineaments picked from potential fields data. The potential fields in parts a and b data are
675 reproduced from Figure 5a and 5b for ease of comparison. Part c shows the interpreted lineaments in
676 the wider study area.

677

678 Figure 14

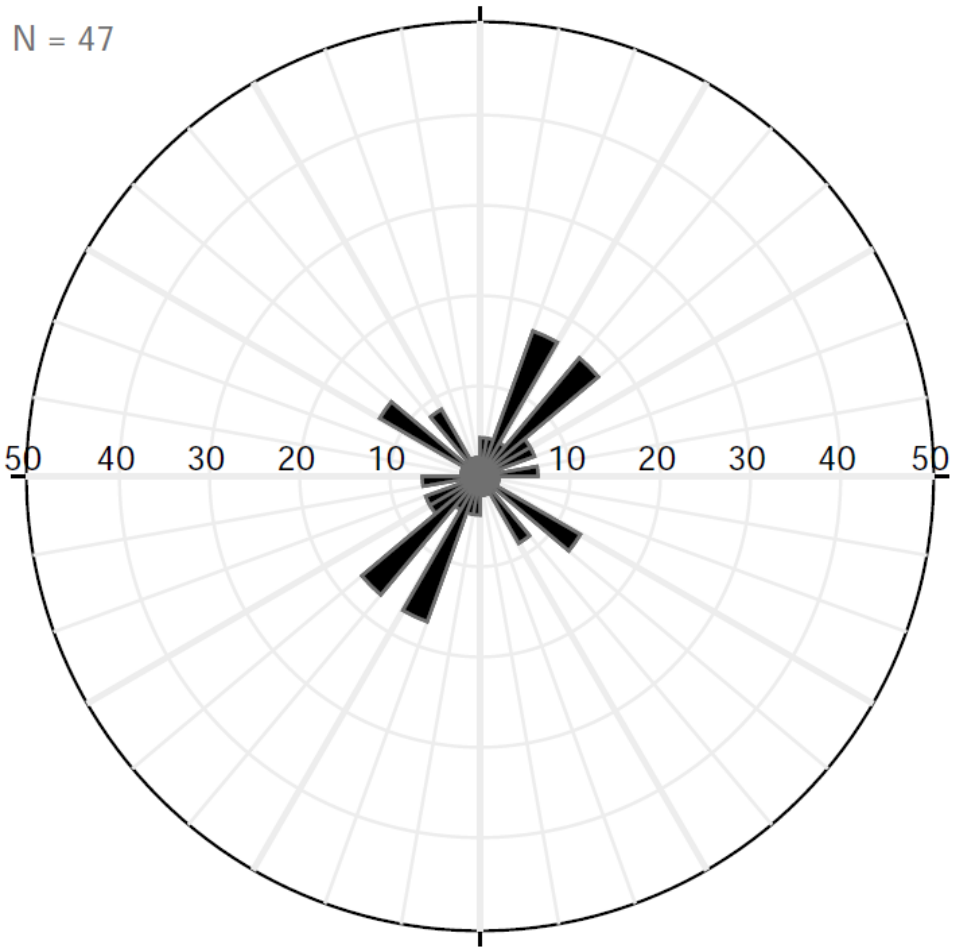

679

680 Figure 14: Rose diagram showing the orientations of all basement lineaments in the study area.

681

682

683

684

685

686

687

688

689

690

691 Figure 15

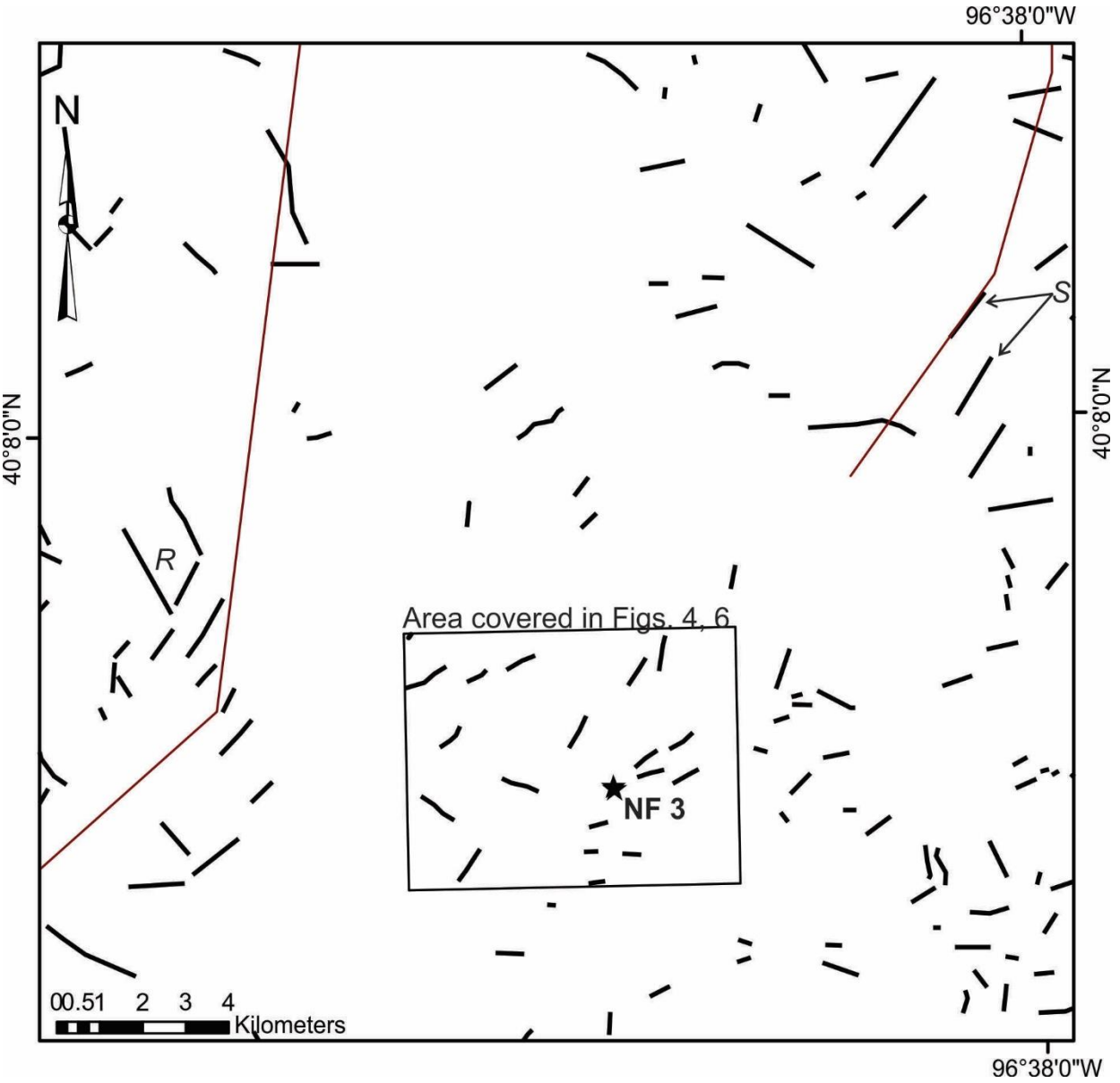

692

693 Figure 15: Map of a subset of the study area, showing basement lineaments (fine red lines) and ETM-
694 derived lineaments. Areas of clear Riedel shears (R) and similar orientations (S and arrows) are labeled.
695 The area covered in Figs 4 and 6, and the location of field site NF 3 are shown for reference.

696